ISSN 1070-4272, Russian Journal of Applied Chemistry, 2015, Vol. 88, No. 1, pp. 178−183. © Pleiades Publishing, Ltd., 2015.

VARIOUS TECHNOLOGIES

Synthesis of the Lead–Calcium HAP Solid Solutions*

Yinian Zhu[a], Zongqiang Zhu[a] , Feng Yang[b], Yanhua Huang[a], and Xin Zhao[c]**

[a] *College of Environmental Science and Engineering, Guilin University of Technology, Guilin, 541004 China*
[b] *College of Environment Engineering, Nanjing Institute of Technology, Nanjing, 211167 China*
[c] *College of Light Industry and Food Engineering, Guangxi University, Nanning, 530004 China*
e-mail: zhuzongqiang@glut.edu.cn

Reveived January 5, 2015

Abstract—A series of lead–calcium hydroxylapatite solid solution was synthesized by the precipitation method. Characterization by various means confirmed the forming of the continuous solid solution over a whole Pb/(Pb+Ca) mole fraction range. An obvious deviation of both *a* and *c* lattice parameters from Vegard's rule was observed. The solids of X_{Pb} = 0–0.51 were typically prism crystals with hexagonal pyramid as a termination (particle size 50–100 nm); those of X_{Pb} = 0.61–0.69 were the typical hexagonal columnar crystals with pinacoid or hexagonal pyramid as termination, which elongated along *c* axis (particle size 200–600 nm); those of X_{Pb} = 0.80–1.00 were the typical prism crystals with hexagonal pyramid as termination (particle size 2–20 μm). The phosphate peak area for the symmetric P–O stretching decreased with increasing Pb/(Pb + Ca) ratio and disappeared as the Pb/(Pb + Ca) ratio > 0.61, and two phosphate peaks of the P–O stretching were diminished with the increase in X_{Pb}. These variations could be caused by a slight tendency of larger Pb^{2+} to prefer the M(II) sites and smaller Ca^{2+} to occupy the M(I) sites in the apatite structure.

DOI: 10.1134/S1070427215010255

INTRODUCTION

Calcium hydroxylapatite (Ca-HAP) is the principal component of vertebral animals' hard tissues and has been widely studied as one of the most important biocompatible materials for coating of bone prostheses and replacement [1–9]. The toxic Pb pollutant may be found in surface and underground waters. When the Pb ions are taken into animals, it is possible that they concentrate in bone through the possible replacement of Ca^{2+} by Pb^{2+} and form the lead-calcium hydroxylapatite solid solution (Pb–Ca-HAP) with vital Ca-HAP. The existence of the toxic metals in animals' hard tissues can cause many bone diseases, such as dental caries and osteoporotic processes [1, 8].

Apatite as the raw material for the phosphate fertilizer industry contains commonly traces of various elements [1]. Additionally, synthetic or natural Ca-HAP from different sources can be used to remove toxic lead ions from industrial wastewaters; this is due to the calcium ion's external position in the HAP structure, which favors an ionic exchange process [1, 9–11]. Particularly, the adsorption of lead by Ca-HAP has been comprehensively investigated because of its extreme toxicity. The reaction of the solid Ca-HAP with lead ions resulted in the forming of hydroxylpyromorphite [$Pb_5(PO_4)_3(OH)$], therewith it should be taken into account that the dissolution of hydroxylapatite is followed with the forming of hydroxylpyromorphite, a solid solution of $Pb_{5-x}Ca_x(PO_4)_3(OH)$ formula, with lead ions generally occupying the M(II) sites [12–15]. From the isomorphism of Ca-HAP and Pb-HAP, the formation of solid solutions among them is considered possible as a result of the simultaneous coupled substitution for Pb in Ca-HAP leading to the formation of solid solutions of $Ca_{5-x}Pb_x(PO_4)_3(OH)$ (Pb–Ca-HAP) [8]. The Pb–Ca-HAP

* The text was submitted by the authors in English.
** The author for correspondence.

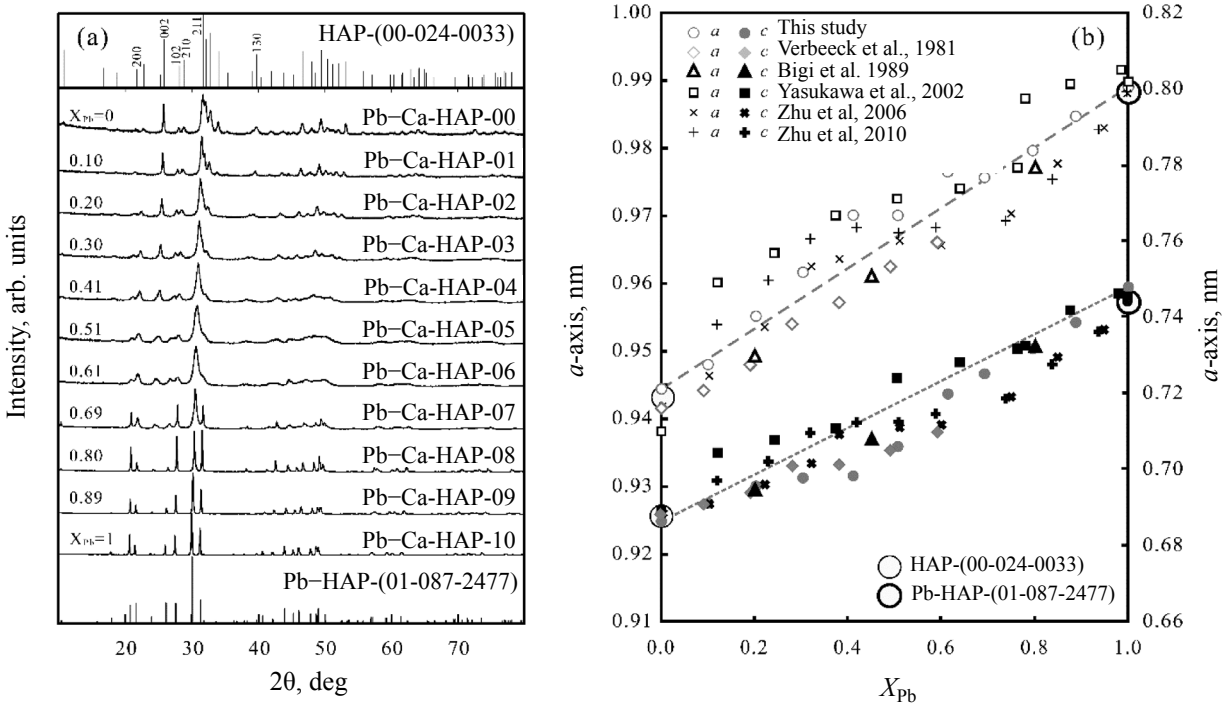

Fig. 1. (a) XRD patterns and (b) lattice parameters of the lead-calcium hydroxyapatite solid solution.

solid solutions have already been prepared by some investigators. They synthesized Pb–Ca-HAP solids by the ion-exchange method, the solid state reaction method and the co-precipitation method. Whereas, in literatures there was a significant difference among the unit cell parameters of the obtained samples, and the previous researches also revealed significant morphological differences [1–3,16–21].

In the present investigation, Pb-HAP, Pb–Ca-HAP and Pb-HAP were synthesized by the precipitation procedure. The obtained solid solution samples were then analyzed by different instruments in detail to study the influence of the Pb molar fraction on the cell parameters and morphology of the Pb–Ca-HAP solid solution with the whole range of the Pb/(Pb + Ca) atomic ratio (X_{Pb}) from 0 to 1, which were synthesized under the same condition of solution pH and temperature.

EXPERIMENTAL

Synthesis. A solutions (250 mL) of various Pb/(Pb + Ca) molar ratios were initially made via dissolving different amounts of $Ca(CH_3COO)_2{\cdot}3H_2O$ and $Pb(CH_3COO)_2{\cdot}H_2O$ into ultrapure water. The amounts of $Ca(CH_3COO)_2{\cdot}3H_2O$ and $Pb(CH_3COO)_2{\cdot}H_2O$ were varied in order to get the synthetic solids with different X_{Pb}, while the total amounts of Pb + Ca were preserved to be 0.4 M. The Pb + Ca solutions were then mixed with 250 mL of 4.4 M CH_3COONH_4 buffer solution in a 1 L polypropylene vessel. Into the vessel 500 mL of 0.12 M $NH_4H_2PO_4$ solution was then quickly added at constant stirring with the formation of white suspensions (see table). The suspension was adjusted to pH 7.5 by adding NH_4OH, stirred for 10 min at room temperature, and aged at 100°C for 48 h. The precipitates were then allowed to settle, washed carefully using pure water, and finally dried in an oven at 70°C for 16 h.

Characterization. Each synthetic solid (10 mg) was firstly dissolved in 20 mL of 1 M nitric acid solution and diluted to 100 mL with pure water. The Ca, Pb, and P contents were then measured by using the inductively coupled plasma, optical emission spectrometer (PE Optima 7000DV). The obtained solid samples were also investigated by the X'Pert PRO powder X-ray diffractometer (XRD) using CuK_α radiation (40 kV and 40 mA) at a scanning rate of 0.10 deg min^{-1} within a 2θ range 10°–80°. The solids were also examined in KBr pellets within 4000–400 cm^{-1} using the Fourier transform infrared spectrophotometer (FT-IR, Nicolet Nexus 470). The morphology was scanned by the field-emission transmission electron microscope (FE-TEM,

Summary of synthesis and composition of the lead-calcium hydroxyapatite solid solution

Sample no.	Volumes of the precursors, mL				Solid composition
	0.4 M $Pb(CH_3COO)_2{\cdot}2H_2O$	0.4 M $Ca(CH_3COO)_2{\cdot}H_2O$	4.4 M CH_3COONH_4	0.12 M $NH_4H_2PO_4$	
Pb-Ca-HAP-00	0	250	250	500	$(Ca_{1.00}Pb_{0.00})_5(PO_4)_3OH$
Pb-Ca-HAP-01	25	225	250	500	$(Ca_{0.90}Pb_{0.10})_5(PO_4)_3OH$
Pb-Ca-HAP-02	50	200	250	500	$(Ca_{0.80}Pb_{0.20})_5(PO_4)_3OH$
Pb-Ca-HAP-03	75	175	250	500	$(Ca_{0.70}Pb_{0.30})_5(PO_4)_3OH$
Pb-Ca-HAP-04	100	150	250	500	$(Ca_{0.59}Pb_{0.41})_5(PO_4)_3OH$
Pb-Ca-HAP-05	125	125	250	500	$(Ca_{0.49}Pb_{0.51})_5(PO_4)_3OH$
Pb-Ca-HAP-06	150	100	250	500	$(Ca_{0.39}Pb_{0.61})_5(PO_4)_3OH$
Pb-Ca-HAP-07	175	75	250	500	$(Ca_{0.31}Pb_{0.69})_5(PO_4)_3OH$
Pb-Ca-HAP-08	200	50	250	500	$(Ca_{0.20}Pb_{0.80})_5(PO_4)_3OH$
Pb-Ca-HAP-09	225	25	250	500	$(Ca_{0.11}Pb_{0.89})_5(PO_4)_3OH$
Pb-Ca-HAP-10	250	0	250	500	$(Ca_{0.00}Pb_{1.00})_5(PO_4)_3OH$

Jeol JEM-2100F) and the field-emission scanning electron microscope (FE-SEM, Hitachi S-4800).

RESULTS AND DISCUSSION

Chemical Compositions

The gained crystals had nearly the planned composition of $(Pb_xCa_{1-x})_5(PO_4)_3(OH)$ (see table). Their experimental (Pb+Ca)/P molar ratios were near the stoichiometric proportion of 1.67 and all the prepared solids were of nearly the same X_{Pb} proportions as the initial solutions.

XRD. The XRD patterns revealed that all the solids belonged to apatite group and crystallized in the hexagonal system $P6_3/m$ varying merely in peak location, absolute intensity, and peak width (Fig. 1a). The solid products with $X_{Pb} = 0$ and 1.00 were recognized as Ca-HAP (Reference code 00-024-0033) and Pb-HAP (Reference code 01-087-2477), respectively. The reflections of Pb–Ca-HAP shifted slowly to a higher-angle direction when X_{Pb} decreased, which showed that Pb–Ca-HAP was a continuous solid solution in all range of $X_{Pb} = 0$–1.00, but it was also indicated in literature that the peaks did not shift in the middle composition of the solid solutions [3, 22]. The replacement of Pb^{2+} for Ca^{2+} could modify the lattice parameters *a* and *c* that increased with the substitution of Pb^{2+}, and an obvious deviation of both *a* and *c* parameters from Vegard's rule was also observed for Pb–Ca-HAP. With increasing X_{Pb}, the lattice parameters *a* and *c* increased from 0.944 to 0.989 nm and from 0.686 to 0.748 nm (Fig. 1b), because of the replacement of Ca^{2+} (0.100 nm) with larger Pb^{2+} (0.119 nm) in the apatite structure [1, 3, 22].

There was a small but significant difference among the unit cell parameters of Pb-HAP, Pb–Ca-HAP, and Ca-HAP in literature (Fig. 1b) [6–12]. Some results showed that the linear variation of the *a*- and *c*-axis dimensions followed Vegard's law over the whole compositional range, i.e., both of them changed linearly with composition between those of the pure end members [17, 19]. Pb^{2+} can replace Ca^{2+} in the apatite lattice in the whole composition range and be distributed randomly in the M(I) and M(II) sites resulting in the linear increasing of the cell parameters. Although some previous investigations reported that the lattice constants varied linearly with X_{Pb}, their data were located only in the range $0 < X_{Pb} < 3$ of the formula $Ca_{5-x}Pb_x(PO_4)_3(OH)$ (Fig. 1b). Since their prepared samples with $X_{Pb} > 3$ comprised great quantities of other lead phosphates, which were not studied further [23].

On the contrary, deviations of the unit cell parameters markedly from Vegard's law have also been reported in literatures [1, 3, 16, 21, 23]. However, the lattice parameters of both *a* and *c* didn't change from X_{Pb} of 0.4 to 0.6 [3, 21], or the change of the *a*-axis parameter had a break at X_{Pb} of 0.8 [1]. These deviations were considered to be the probable preference of Pb^{2+} for the M(II) sites of the

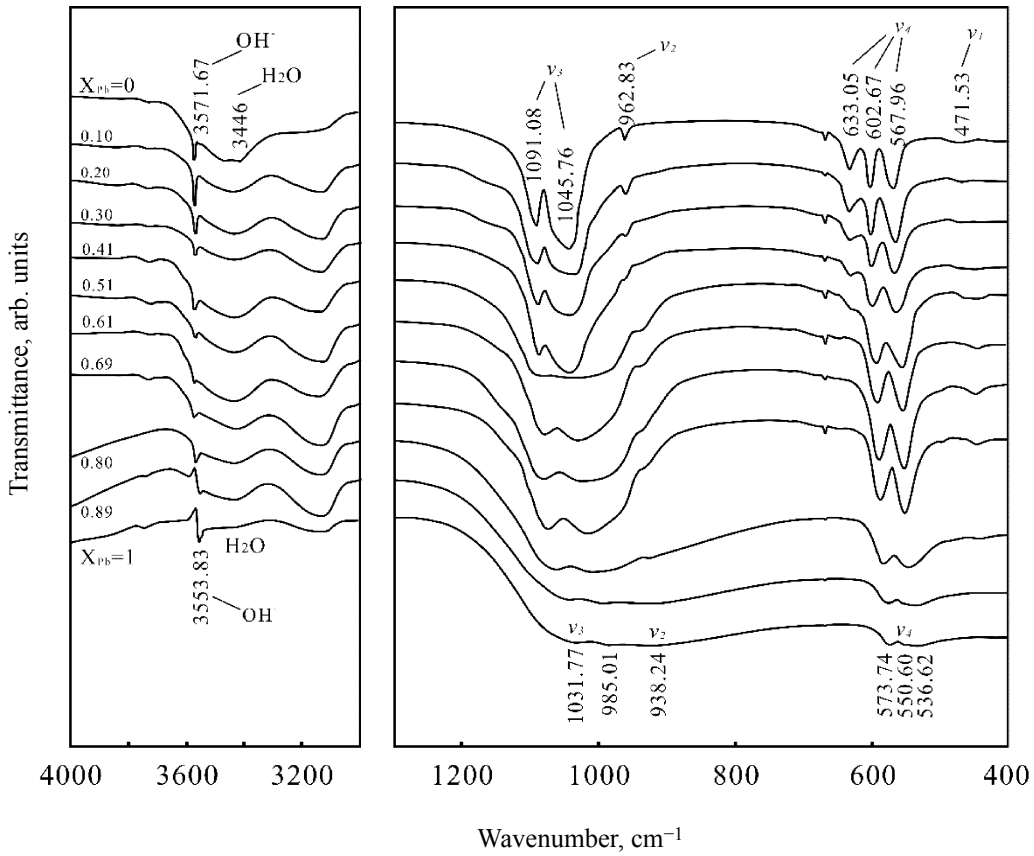

Fig. 2. Fourier transform infrared spectra of the lead-calcium hydroxyapatite solid solution.

apatite lattice, i.e., the six fold positions of the cation sublattices [16]. The greatest deviations were noted at an intermediate X_{Pb}, whereas the entire replacement of Pb^{2+} formed a crystal of the apatite structure, despite a total enlargement of the unit cell because of the larger Pb^{2+} [3, 19–24]. When Pb^{2+} substituted for Ca^{2+} in the apatite lattice, it occupied almost solely the M(II) sites, until, at $X_{Pb} > 0.4$, it also began to occupy the M(I) site considerably, which could explain the discontinuity at around $X_{Pb} = 0.4–0.6$ in the curves of the *a* and *c*-axis parameters versus X_{Pb} (Fig. 1b). The replacement of Pb^{2+} for Ca^{2+} in the M(I) sites, i.e., in the columns parallel to the *c* axis, can result in a greater enlargement of the *c*-axis parameter than that provoked by Pb^{2+} replacement in the M(II) sites. In the apatite lattice, the M(II)–M(II) length are greater than the M(I)–M(I) length, thus the former doesn't vary significantly up to $X_{Pb} \approx 0.4$, while the M(I)–M(I) length can be intensely influenced even if a little amount of Pb^{2+} exists [3, 19–22].

FTIR. For the tetrahedral phosphate ion, there are four normal peaks, i.e., the symmetric P–O stretching (ν_1), the OPO bending (ν_2, ν_4), and the P–O stretching (ν_3) [2]. In the recorded FTIR spectrum, the essential vibrational peaks of PO_4^{3-} tetrahedra for Ca-HAP were observed in the region around at 962.83 cm^{-1} (ν_2), 1045.76 and 1091.08 cm^{-1} (ν_3), 567.96 and 602.67 cm^{-1} (ν_4), which shifted to 938.24 cm^{-1} (ν_2), 985.01 and 1031.77 cm^{-1} (ν_3), 536.62–573.74 cm^{-1} (ν_4) as X_{Pb} increased from 0 to 1.00, respectively (Fig. 2). The bands at 471.53 cm^{-1} (ν_1) and 633.05 cm^{-1} (ν_4) decreased with increasing X_{Pb} and disappeared as $X_{Pb} > 0.80$ due to a change in the symmetry of PO_4^{3-}. All the bands, especially for the two P–O stretching (ν_3) peaks, were diminished with the increase in X_{Pb} because of the scattering of IR beam by large particles observed in the FE-SEM and TEM images (Fig. 3) [1].

The spectra of all solid samples showed a strong sharp band at 3553.83–3571.67 cm^{-1}, which represented the stretching vibrations of the bulk OH^-, but it was not observed that the OH^- band was shifted from 3571.67 to 3553.83 cm^{-1} with the increasing X_{Pb} from 0 to 1.00 as reported in the literature [8, 24]. The band at 3735.15–3736.56 cm^{-1} represented the surface P–OH groups. The band at 871 cm^{-1} for HPO_4^{2-} [1, 9] and the band at

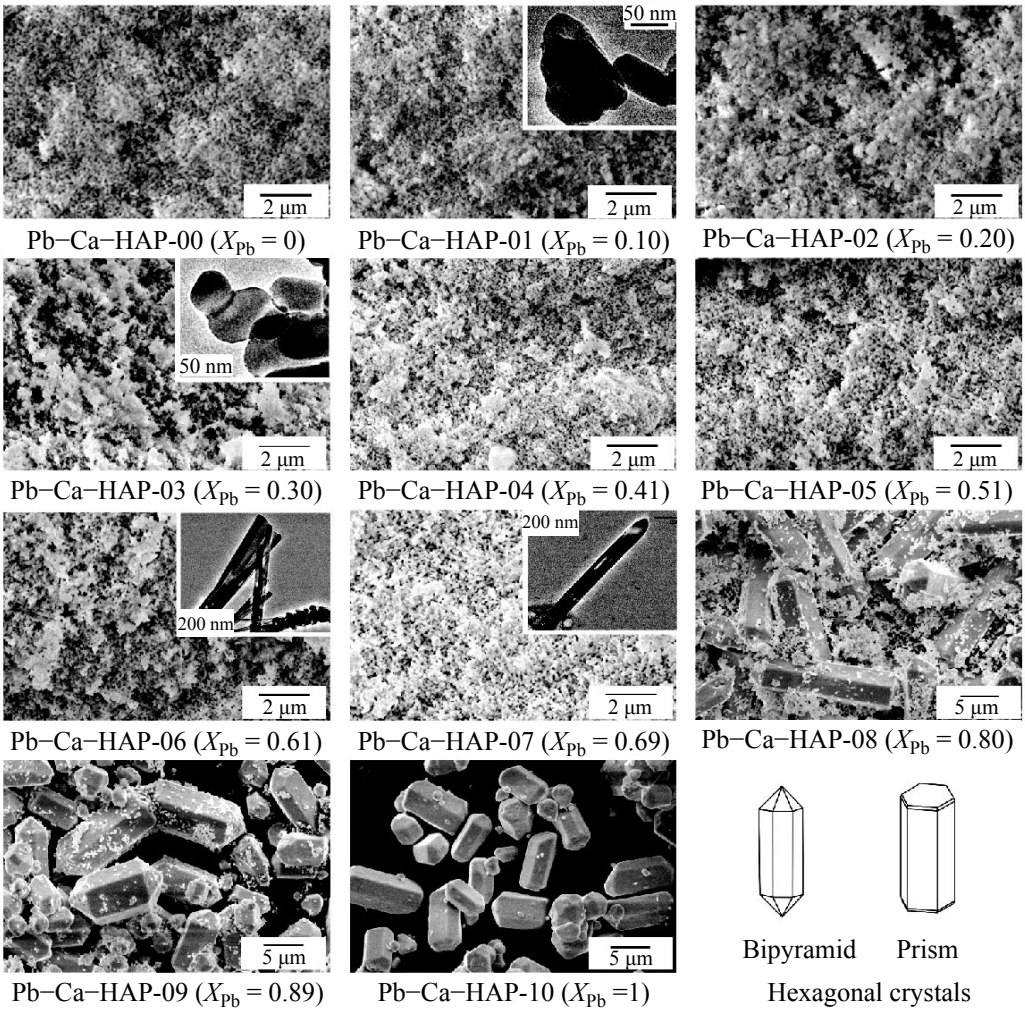

Fig. 3. Field emission scanning electron micrographs and transmission electron microscope images and hexagonal crystals of the lead-calcium hydroxyapatite solid solution.

1455 cm^{-1} for CO_3^{2-} vibration [25] were not obviously detected in the spectra (Fig. 2).

FE-SEM and TEM. The crystal structure and morphology of the prepared solids were affected by the Pb/(Pb + Ca) atomic ratio [1, 3, 22]. With increasing X_{Pb}, the unit cell parameters increased gradually accompanying morphology variation (Fig. 3). The solids of X_{Pb} = 0–0.51 were typically prism crystals with the hexagonal pyramid as a termination (particle size 50–100 nm); those of X_{Pb} = 0.61–0.69 were the typical hexagonal columnar crystals with pinacoid or hexagonal pyramid as a termination, which elongated along *c* axis (particle size 200–600 nm); those of X_{Pb} = 0.80–1.00 were the typical prism crystals with the hexagonal pyramid as a termination (particle size 2–20 μm). The crystal sizes decreased slightly with increasing X_{Pb} from 0.80 to 1.00. This finding was different from the previous research, which showed that the particles were well-crystalline needle-like and grew with increasing X_{Pb} [1]. The solid solution mean crystal size along the hydroxyapatite (300) and (002) directions increased with increasing X_{Pb} since Pb^{2+} ions preferentially occupy the M(II) sites [26].

CONCLUSIONS

The obtained lead-calcium hydroxylapatite solid solution (Pb–Ca-HAP) showed the apatite structure. With the increase of X_{Pb}, the unit cell *a* and *c* parameters increased from 0.944 to 0.989 nm and from 0.686 to 0.748 nm, respectively, but an obvious deviation of both *a* and *c* lattice parameters from Vegard's rule was observed. The peak positions of the symmetric P–O stretching and the

OPO bending decreased with the increasing of X_{Pb}; the two peaks of the P–O stretching (v_3) were diminished with the increase of X_{Pb}. The particles changed from smaller prism crystals (X_{Pb} = 0–0.51) to larger hexagonal columnar crystals (X_{Pb} = 0.61–0.69) and then to larger prism crystals (X_{Pb} = 0.80–1.00). These variations could be caused by the slight tendency of larger Pb^{2+} to preferentially occupy the M(II) sites and of smaller Ca^{2+} to occupy the M(I) sites in the apatite structure.

ACKNOWLEDGMENTS

The manuscript has greatly benefited from the editor and anonymous reviewer insightful comments. The authors thank the financial supports from the National Natural Science Foundation of China (41263009), the Special Funding for Guangxi "BaGui Scholars" Construction Projects, the Provincial Natural Science Foundation of Guangxi (2012GXNSFDA053022), and the Guangxi Science and Technology Development Project (Gui Ke Zhong 1298002-3).

REFERENCES

1. Yasukawa, A., Kamiuchi, K., Yokoyama, T., and Ishikawa, T., *J. Solid State Chem.,* 2002, vol. 163, pp. 27–32.
2. Zhu, K. Yanagisawa, A. Onda, K. Kajiyoshi, and Qiu, J., *Mater. Chem. & Phys.,* 2009, vol. 113, pp. 239–243.
3. Zhu, K., Qiu, J., Ji, H., Yanagisawa, K., Shimanouchi, R., Onda, A., and Kajiyoshi, K., *Inorg. Chim. Acta,* 2010, vol. 363, pp. 1785–1790.
4. Chahal, S., Hussain, F.S.J., and Yusoff, M.B.M., *Bio-Med. Mater. & Eng,* 2014, vol. 24, pp. 799–806.
5. Yang, M., Shuai, Y., Zhou, G., Mandal, N., and Zhu, L., *Bio-Med. Mater. & Eng,* 2014, vol. 24, pp. 731–740.
6. Yang, M., Mandal, N., Shuai, Y., Zhou, G., Min, S., and Zhu, L., *Bio-Med. Mater. & Eng,* 2014, vol. 24, pp. 815–824.
7. Ben Cherifa, A., Jemal, M., Nounah, A., and Lacout, J.L., *Thermochimica Acta,* 1994, vol. 237, pp. 285–293.
8. Mahapatra, P.P., Sarangi, D.S., and Mishra, B., *J. Solid State Chem.,* 1995, vol. 116, pp. 8–14.
9. Yasukawa, A., Higashijima, M., Kandori, K., and Ishikawa, T., *Colloids & Surface A,* 2005, vol. 268, pp. 111–117.
10. Piccirillo, C., Pereira, S.I.A., Marques, A.P.G.C., Pullar, R.C., Tobaldi, D.M., Pintado, M.E., and Castro, P.M.L., *J. Env. Manag.,* 2013, vol. 121, pp. 87–95.
11. Evis, Z., Yilmaz, B., Usta, M., and LeventAktug, S., *Ceramics Int.,* 2013, vol. 39, 2359–2363.
12. Arnich, N., Lanhers, M.C., Laurensot, F., Podor, R., Montiel, A., and Burnel, D., *Env. Pollution,* 2003, vol. 124, pp. 139–149.
13. Bailliez, S., Nzihou, A., BuChe, E., and Flamant, G., *Process Safety & Env. Protect.,* 2004, vol. 82, pp. 175–180.
14. Jang, S.H., Jeong, Y.G., Min, B.G., Lyoo, W.S., and Lee, S.C., *J. Hazar. Materials,* 2008, vol. 159, pp. 294–299.
15. Dong, L., Zhu, Z., Qiu, Y., and Zhao, J., *Chem. Eng. J.,* 2010, vol. 165, pp. 827–834.
16. Engel, G., Krieg, F., and Reif, G., *J. Solid State Chem.,* 1975, vol. 15, pp. 117–126.
17. Heijligers, H.J.M., Driessens, F.C.M., and Verbeeck, R.M.H., *Calcified Tissue Int.,* 1979, vol. 29, pp. 127–131.
18. Sugiyama, S., Minami, T., Moriga, T., Hayashi, H., and Moffat, J.B., *J. Solid State Chem.,* 1998, vol. 135, pp. 86–95.
19. Bigi, A., Ripamonti, A., Bruckner, S., Gazzano, M., Roveri, N., and Thomas, S.A., *Acta Crystallograph.,* 1989, vol. B45, pp. 247–251.
20. Bigi, A., Gandolfi, M., Gazzano, M., Ripamonti, A., Roveri, N., and Thomas, S.A., *J. Chem. Soc., Dalton Trans.,* 1991, vol. 11, pp. 2883–2886.
21. Zhou, J.Z., Xu, X., Zhang, Y., and Qian, G.R., *J. Inorg. Mater.,* 2009, vol. 24, pp. 259–263.
22. Zhu, K., Yanagisawa, K., Shimanouchi, R., Onda, A., and Kajiyoshi, K., *J. Europ. Ceram. Soc.,* 2006, vol. 26, pp. 509–513.
23. Verbeeck, R.M.H., Lassuyt, C.J., Heijligers, J.M., Driessens, C.M., and Vrolijk, J.W.G.A., *Calcified Tissue Int.,* 1981, vol. 33, pp. 243–247.
24. Bruckner, S., Lusvardi, G., Menabue, L., and Saladini, M., *Inorg. Chim. Acta,* 1995, vol. 236, pp. 209–212.
25. Qian, G., Bai, H., Sun, F., Zhou, J., Sun, W., and Xu, X., *J. Inorg. Mater.,* 2008, vol. 23, pp. 1016–1020.
26. Mavropoulosa, E., Rochab, N.C.C., Moreirac, J.C., Rossia, A.M., and Soares, G.A., *Materials Characterization,* 2004, vol. 53, pp. 71–78.